



Study on the Mechanical and Corrosion behavior of AA5052 Tailor Welded Blanks Fabricated using Friction Stir Welding

A. Yukesh Aravind, R. Vaira Vignesh, R. Padmanaban, M. Govindaraju

Department of Mechanical Engineering, Amrita School of Engineering, Coimbatore, Amrita Vishwa Vidyapeetham, India.

Received 22 June 2019,
Revised 231 July 2019,
Accepted 26 July 2019

Keywords

- ✓ Friction Stir Welding,
- ✓ Tailor Welded Blanks,
- ✓ Tensile Strength,
- ✓ Microhardness,
- ✓ RBG.

dr_padmanaban@cb.amrita.edu ;
Phone: 9487368309

Abstract

Friction stir welding is a unique and promising technique to produce joints with desirable mechanical strength and properties. Tailor welded blanks are processed by joining two plates of dissimilar thickness with relatively less mass. As tailor welded blanks offer higher strength at a minimal weight, the material consumption decreases making it more economically viable. In this study, the influence of the critical friction stir welding process parameters namely tool traverse speed, tool rotation speed and thickness mismatch ratio on the microhardness, corrosion rate, tensile strength (before and after corrosion) of AA5052 tailor welded blanks are investigated. The friction stir welding trials were conducted based on Box Behnken design at three levels of process parameters. Hybrid-Radial Basis Function based models were developed to explore the effect of process parameters on the properties. The optimum process parameters to obtain high tensile strength in AA5052 tailor welded blanks was found to be tool traverse speed of 60mm/min, the tool rotation speed of 850rpm and thickness mismatch ratio of 0.9.

1. Introduction

Aluminum is the third most abundant material available in the earth's crust and is unique because of its low density. Accordingly, aluminum and its alloys are extensively used in aerospace, transportation, and marine applications [1]. Of the many properties, the rapid reaction of aluminum with atmospheric oxygen forming oxides cause serious problems in conventional welding [2]. Besides, thermal cracking, porosity in the region of fusion, and reduced joint are some of the common problems that are encountered during conventional welding of aluminum alloys [3-5]. Hence, the solid-state joining of aluminum alloys has become an extensive area of research. The Welding Institute, Cambridge, England, developed friction Stir Welding (FSW). It is a vital joining technique to join engineering components made of aluminum alloys [6, 7].

FSW uses a non-consumable rotating tool that traverses along the joint line under the action of the load to enable weldment between the workpieces. The frictional heat generated between the tool and the workpiece deforms the material plastically and enables dynamic recrystallization [8, 9]. This enables a weld zone with low distortion level and residual stress level, as no melting is involved [10, 11]. A tailor welded blank (TWB) is produced by joining two or more sheets of similar or dissimilar materials, which differ in grade, gauge, and coating [12-14]. Introducing the concept of TWB for aluminum alloys seemed nearly impossible until FSW made its way. AA5052 alloy (Al-Mg alloy system, with the primary alloying element as Mg) is conventionally used in automotive and marine applications [15-17]. The need for joining metal-alloy sheets of various thickness in the present-day automotive structures necessitates investigation on the fabrication of AA5052 tailor welded blanks. Optimum welding parameters are essential to obtain sound joints [18, 19]. A brief literature survey on the friction stir welding of AA5052 alloy is given in the following section.

Mishra et al., [6, 8] reviewed the significant advantages of FSW of aluminum alloys. Chanakyan et al., [20] correlated the microstructure with the mechanical properties of AA5052 alloy that was FSWed at various process parameters (tool rotation speed, tool traverse speed, tool pin profile). Xiangbin et al., [15] presented a brief review of the FSW of dissimilar Al/Al and Al/Non-Al alloys. The literature survey indicates a persistent gap in utilizing the FSW process for fabricating TWB in AA5052 alloy.

In this study, AA5052 alloy of various thickness was joined by FSW process. The FSW trials were performed at various process parameters (tool rotation speed, tool traverse speed, thickness mismatch ratio) that were varied based on Box Behnken Design. The welded specimens were characterized for defects, microhardness, corrosion rate, and tensile strength. Hybrid quadratic – radial basis function models were developed to interrelate the process parameters with the properties. The developed and validated models were used to generate contour plots. The study presents a comprehensive analysis of the influence of process parameters on the properties of the joint using the generated contour plots. Besides, the fractography and surface morphology analysis were presented to describe the fracture and corrosion mechanism of the joints.

2. Materials and Methods

2.1. Materials

Wrought AA5052 alloy of thickness 4 mm was chosen as the base material. The melting point of AA5052 is 650°C, and the tensile strength is 190 MPa [21]. The chemical composition of AA5052 alloy is given in Table 1. The wrought plate was cut into workpieces of dimension 150 mm × 58 mm. The thickness was reduced to 3.2 mm in a few plates and 3.6 mm in a few plates. The plates were ensured for flatness after machining operation.

Table 1: Chemical Composition of AA5052 alloy

| Chemical Composition | Mg | Cr | Cu | Fe | Mn | Si | Zn | Al |
|----------------------|------|-------|------|------|------|-------|------|---------|
| Weight Percentage | 2.6% | 0.28% | 0.1% | 0.4% | 0.1% | 0.25% | 0.1% | Balance |

2.2. Friction Stir Welding

The FSW trials were performed by varying the process parameters tool rotation speed (TRS), tool traverse speed (TTS), thickness mismatch ratio (TMR) at 3 levels. The selected range of process parameters from the literature is given in Table 2. The Box Behnken Design based experimental layout is given in Table 3. The workpieces were held firm in a mild steel backing plate using a dedicated fixture to restrain any vibrations that were generated during FSW. The FSW tool was made of High Carbon High Chromium Steel, with a pin diameter of 4 mm, pin height (3.2 mm, 3.6 mm, 4.0 mm) and shoulder diameter of 18 mm. FSW trials were performed using a dedicated Friction Stir Welding setup at Amrita Vishwa Vidyapeetham.

Table 2: Friction stir welding process parameters

| Sl. No. | TRS (rpm) | TTS (mm/min) | TMR | Coded Value |
|---------|-----------|--------------|-----|-------------|
| 1 | 750 | 20 | 0.8 | -1 |
| 2 | 900 | 40 | 0.9 | 0 |
| 3 | 1000 | 60 | 1 | 1 |

2.3. Microhardness Test

The cross-section of the welded specimens along weld nugget zone (WNZ), thermo-mechanically affected zone (TMAZ) and base material (BM) was subjected to microhardness testing at 10 equidistant points using Vicker's Microhardness testing machine. The testing was done in line with standard ASTM E384. The indentations were performed using a diamond indenter with 100gf load, which was applied for 15s. The microhardness was obtained using the cross diagonal length of the indentation using dedicated software.

2.4. Nitric Acid Mass Loss Test

The nitric acid mass loss test (NAMLT) was conducted to determine the susceptibility of the AA5052 alloy and FSWed specimens to intergranular corrosion, as per the standard ASTM G67-18. The specimens were cleaned using acetone and were placed in a closed-conical flask containing nitric acid solution at room temperature for 24 hours. The conical flasks were placed in a thermostatic water bath to maintain the temperature. The mass of the specimens before and after NAMLT was measured using a precision weighing balance with a readability of 0.0001 g. The details of the test could be found in our earlier research works [3, 16].

2.5. Tensile Test

The tensile test specimens were prepared, and the tensile test was performed as outlined by the standard ASTM B557-1. The dimensions of the tensile test specimens were as follows: gauge length of 25 mm; grip length of 25 mm; and corresponding thickness.

The tensile test was performed on a computerized universal testing machine at a crosshead speed of 0.5mm min⁻¹. The average tensile strength of three tensile test specimens is reported in the study. The tensile test was conducted after NAMLT test to study the influence of corrosion on the tensile strength of the FSWed joints.

2.6. Quadratic – Radial Basis Function Model

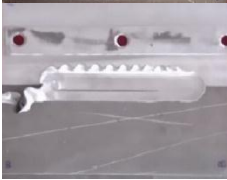
A hybrid quadratic – radial basis function model was developed to correlate the process parameters (TRS, TTS, TMR) with the properties. The details on the development of models are discussed in our earlier research works [3, 22-24]. The statistical parameters namely root mean squared error (RMSE), coefficient of determination (R²) and adjusted R² model were used to assess the effectiveness of the developed model. The contour plots were obtained from the models to optimize the process parameters.

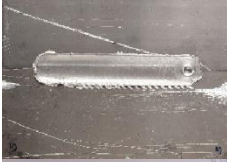
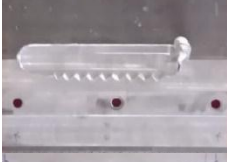
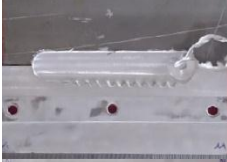
3. Results and discussion

3.1. Defect Analysis

The photograph of the FSWed plates with the corresponding defect is shown in Table 3. Either of the following reasons causes the defects in the joints: less heat generation, high heat generation, turbulent flow of material, and ineffective material transfer. Low TRS and high TTS cause less heat generation, whereas high TRS and low TTS cause high heat generation. High TRS causes turbulent flow of material. Low TTS causes poor material transfer. Specimen A Specimen C, Specimen E, Specimen G, Specimen I, Specimen O had no defects on the surface. Specimen B, Specimen F, Specimen J, Specimen K, Specimen L, Specimen M, and Specimen N exhibited surface lack of fill, which occurs due to improper material transfer and insufficient forge pressure. Surface Galling was observed in the Specimen D and Specimen H, which had a ripped structure on the top surface of the weld.

Table 3: Defect analysis in the tailor welded blanks

| Specimen | TRS (rpm) | TTS (mm/min) | TMR | Photo | Defect |
|----------|-----------|--------------|-----|--|-----------------------|
| A | 1000 | 60 | 1 |  | No defect |
| B | 1000 | 60 | 0.8 |  | Surface Lack of Fill |
| C | 1000 | 20 | 1 |  | No defect |
| D | 1000 | 20 | 0.8 |  | Minor Surface Galling |
| E | 750 | 60 | 1 |  | No defect |
| F | 750 | 60 | 0.8 |  | Surface Lack of Fill |

| | | | | | |
|---|------|----|-----|--|---------------------------------------|
| G | 750 | 20 | 1 |  | No defect |
| H | 750 | 20 | 0.8 |  | Minor Surface Galling |
| I | 900 | 40 | 1 |  | No defect |
| J | 900 | 40 | 0.8 |  | Surface Lack of Fill |
| K | 900 | 60 | 0.9 |  | Surface Lack of Fill |
| L | 900 | 20 | 0.9 |  | Minor Surface Lack of Fill at the end |
| M | 1000 | 40 | 0.9 |  | Surface Lack of Fill |
| N | 750 | 40 | 0.9 |  | Surface Lack of Fill |
| O | 900 | 40 | 0.9 |  | No defect |

3.2. Microhardness

Figure 1 shows the typical microhardness profile of the FSWed specimen A across the nugget region from the base material zone and thermo-mechanically affected zone. It is observed that the microhardness in the nugget zone is relatively lesser than that of the base material. This is caused by the growth and agglomeration of the β phase (Mg_2Al_3) in the nugget zone. Figure 2 shows the average microhardness of the FSWed specimen. Among the FSWed specimens, a maximum microhardness 87.1 HV was observed in the specimen E that was FSWed at TTS of 60 mm/min, TRS of 750 rpm and TMR of 1. This is credited to the refinement of grains and fine dispersion of the β phase in the nugget zone.

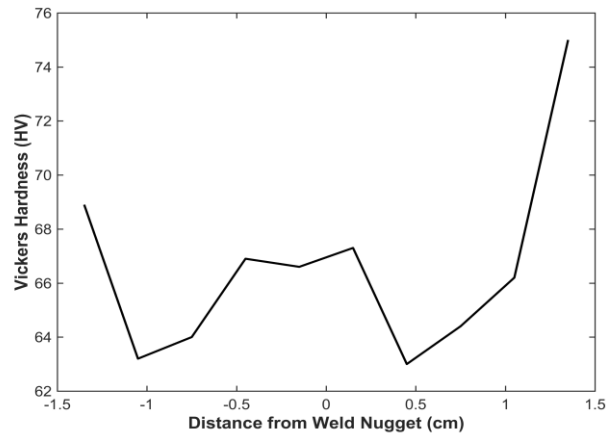


Figure 1: Microhardness of Specimen A

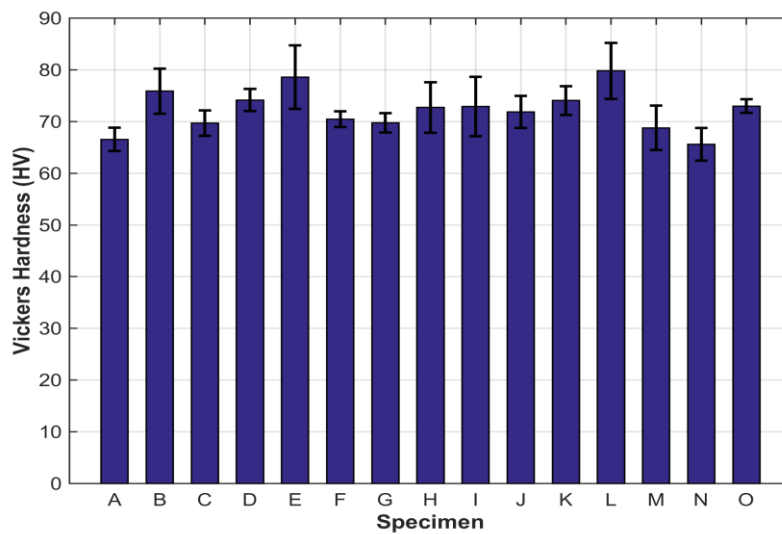


Figure 2: Mean microhardness values for all the specimens

The hybrid model for predicting the microhardness of the friction stir welded specimens is given by the equation (1). The model was used to study the effect of process parameters on the microhardness of the friction stir welded specimens.

$$\text{Microhardness} = 116.3359 - 7.988965 \times \text{TMR} + 5.122361 \times \text{TRS} - 10.87807 \times \text{TTS} + 5.100003 \times \text{TMR}^2 + 2.110971 \times \text{TRS}^2 + 8.40697 \times \text{TTS}^2 + \text{RBF Network using a multiquadric kernel with 4 centres, a global width of 0.082678, and regularization parameter, lambda is 0.0001.} \quad (1)$$

Figure 3 shows the contour graphs generated from the model. From Figure 3a, it is observed that the specimens FSWed at TRS greater than 900 rpm and TMR greater than 0.86 resulted in low microhardness value. The heat input at the joint interface increased with an increase in TRS. This resulted in grain growth and agglomeration of the β phase, which in turn reduced the hardness. FSW of specimens at TRS lesser than 850 rpm and TMR greater than 0.92 resulted in high microhardness value. The optimum heat generation supported dynamic recovery and recrystallization, which eventually decreased the grain size and ensured a fine dispersion of β phase. Hence, the FSW of specimens at TRS lesser than 850 rpm had higher microhardness. Figure 3b shows the influence of TTS and TRS on the microhardness of the FSWed specimens. The graphs indicate that the specimens FSWed at TRS above 900 rpm and TTS in the range of 20 mm/min and 50 mm/min resulted in low microhardness. The low TTS and high TRS combination favored excessive heat generation, which coarsened the grains and agglomerated the β phase [25-27]. This reduced the microhardness of the specimens. However, optimum heat generation coupled with dynamic recovery and recrystallization in the specimens FSWed at TRS below 850 rpm and TTS above 57 mm/min resulted in high microhardness value.

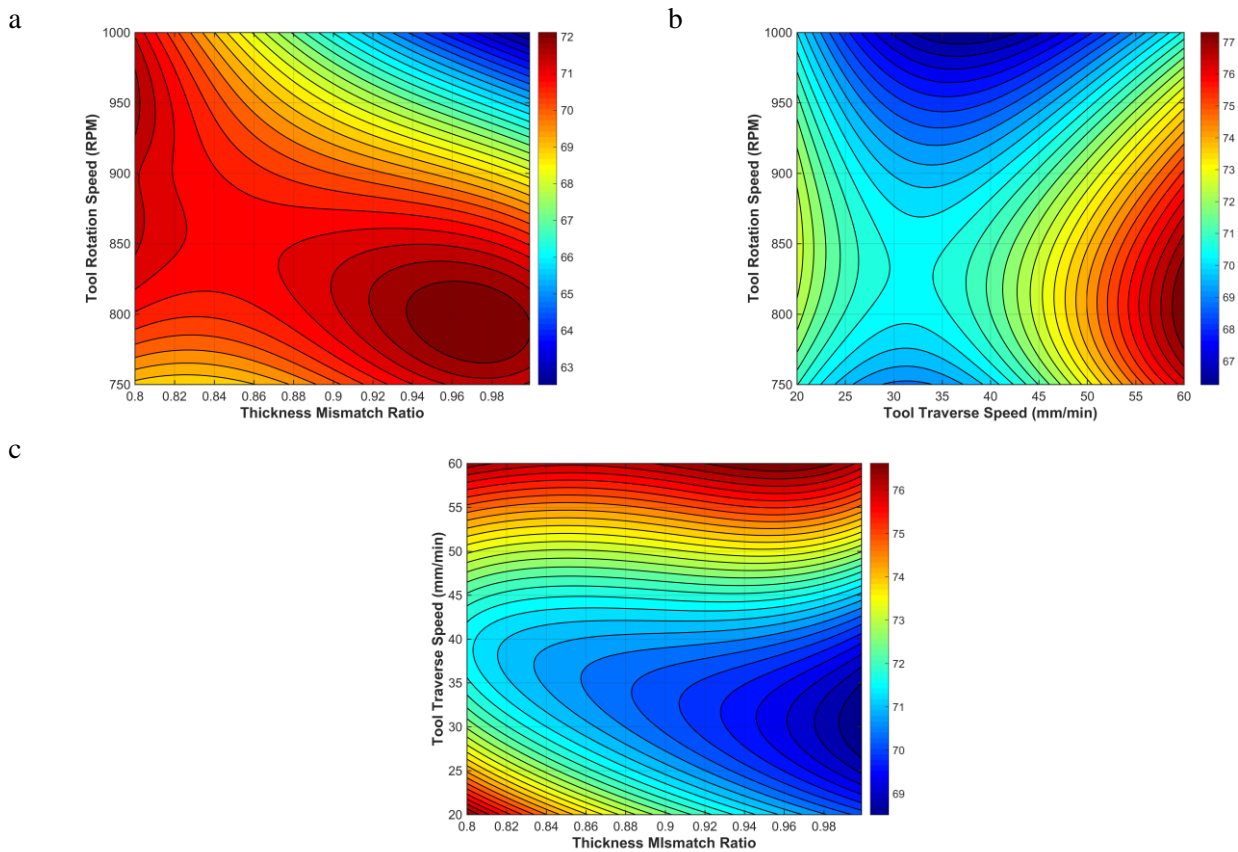


Figure 3: Contour plots showing the effect of a) TRS & TMR b) TRS & TTS and c) TTS & TMR on Microhardness

As shown in Figure 3c, FSW of specimens in the TTS between of 25 mm/min and 40 mm/min, and TMR above 0.9 resulted in low microhardness value, while TTS above 55mm/min and TMR ranging between 0.92 - 1 results in high microhardness value. This is consistent with the relation between heat generation and coarsening of grains and agglomeration of the β phase, as indicated earlier. The optimum range of FSW process parameters that were inferred from the contour plots are as follows: TRS between 750 rpm and 850 rpm; TTS between 57 mm/min and 60 mm/min; TMR between 0.92 – 1. The maximum microhardness that could be obtained by FSW at this level of process parameters would be 72 HV – 76 HV.

3.3. Nitric Acid Mass Loss Test

The NAMLT test was performed to assess the intergranular corrosion susceptibility of the FSWed specimens. The preferential dissolution of β phase by nitric acid results in a mass loss in the FSWed specimens. The mass loss per unit area of the specimens after 24 hours of immersion in nitric acid is shown in Table 4. A higher mass loss per unit area indicates more precipitation of β phase in the matrix, whereas a lower mass loss per unit area indicates fine dispersion and partial dissolution of the β phase in the matrix. As per the guidelines of the standard, a mass loss of less than 15 mg/cm² indicates intergranular corrosion-resistant material and a mass loss of above 25 mg/cm² indicates intergranular corrosion-prone material. A maximum mass loss per unit area of 10.729 mg/cm² was observed for the specimen N, which was processed at TRS of 750 rpm, TTS of 40 mm/min and TMR of 0.9. It is observed that the mass loss was very minimal (around 1.35%), which indicated that all the FSWed specimens were not susceptible to intergranular corrosion. The hybrid model for predicting the mass loss per unit area of the FSWed specimens is given by equation (2).

$$\text{Mass loss per unit area} = 11.5892 + 1.172529 \times \text{TRS} - 2.13924 \times \text{TTS} - 2.52093 \times \text{TMR} + 0.909187 \times \text{TRS}^2 - 1.05897 \times \text{TTS}^2 - 2.25034 \times \text{TMR}^2 + \text{RBF Network using a multiquadric kernel with 5 centers, and a global width of 0.17593, and regularization parameter, lambda is 0.0001.} \quad (2)$$

The developed model was used to study the effect of process parameters on the mass loss per unit area of the FSWed specimens. As shown in Figure 4a, FSW of specimens at TRS ranging from 750 rpm to 800 rpm / 950 rpm to 1000 rpm and for any TMR results in high mass loss per unit area. However, specimens FSWed at TRS between 800 rpm and 950 rpm, and TMR less than 0.82 results in low mass loss per unit area. A similar trend was

observed between TTS and TRS for mass loss per unit area in the FSWed specimens, as exposed in Figure 4b. FSW of the specimen at TRS less than 800 rpm / more than 950 rpm and for any TTS results in less mass loss per unit area, whereas TRS between 850 rpm and 950 rpm and for any TTS results in low mass loss per unit area. As shown in Figure 4c, FSW of specimens above 55 mm/min and TMR less than 0.84 / more than 0.96 results in less mass loss per unit area. But, FSW of specimens at TTS ranging from 30 mm/min to 50 mm/min and TMR ranging between 0.92 to 0.96 results in high mass loss per unit area.

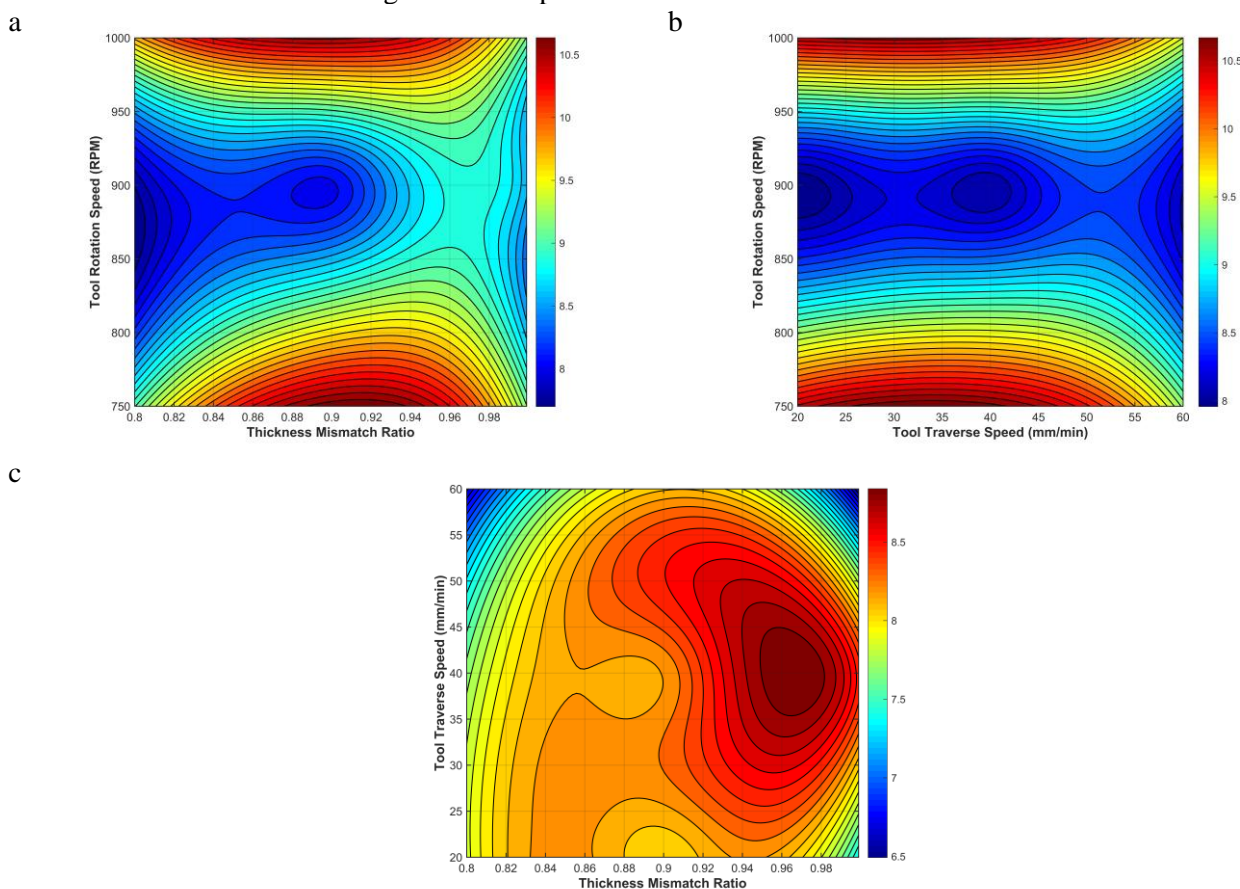


Figure 4 Contour plots showing the effect of a) TRS & TMR b) TRS & TTS and c) TTS & TMR on mass loss per unit area

The optimum range of FSW process parameters that were inferred from the contour plots are as follows: TRS between 800 rpm and 950 rpm; TTS between 55 mm/min and 60 mm/min; TMR between 0.96 – 1. The mass loss per unit area that could be obtained by FSW at this level of process parameters would be 8 mg/cm² – 8.5 mg/cm². The surface morphology of the FSWed specimen D was observed in a Field Emission Scanning Electron Microscope (FESEM) after NAMLT.

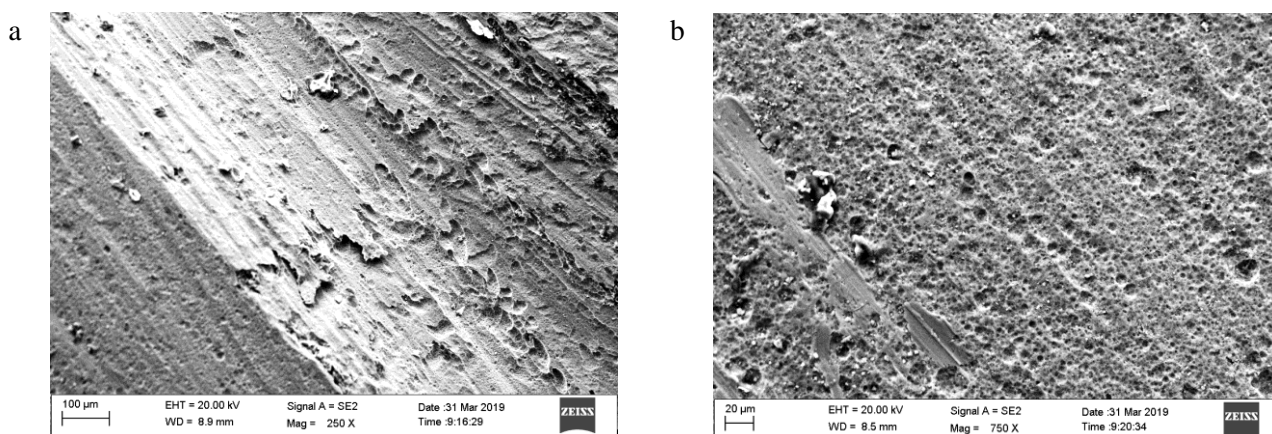


Figure 5 Surface morphology analysis a) Interface of base material and weld zone; b) Magnified view of base material

Figure 5a and Figure 5b indicate pitting phenomenon in the base material. Characteristic exfoliation was observed in the weld region, as shown in Figure 5a.

3.4. Tensile Strength

The average tensile strength (TS) of the FSWed specimens before and after NAMLT test are shown in Table 4. Specimen L that was FSWed at TTS of 20 mm/min, TRS of 900 rpm and TMR of 0.9 exhibited the highest TS before and after NAMLT.

Table 4: Experimental layout and its corresponding results

| Specimen | TRS (rpm) | TTS (mm/min) | TMR | Microhardness (HV) | Mass loss per unit area (mg/cm ²) | Tensile Strength - before NAMLT (MPa) | Tensile Strength - after NAMLT (MPa) |
|----------|-----------|--------------|-----|--------------------|---|---------------------------------------|--------------------------------------|
| A | 1000 | 60 | 1 | 65.95 | 7.186 | 119.13 | 112.44 |
| B | 1000 | 60 | 0.8 | 78.87 | 8.453 | 40.89 | 32.45 |
| C | 1000 | 20 | 1 | 67.02 | 8.891 | 121.18 | 115.90 |
| D | 1000 | 20 | 0.8 | 76.02 | 10.054 | 37.89 | 25.01 |
| E | 750 | 60 | 1 | 87.10 | 7.822 | 125.51 | 124.64 |
| F | 750 | 60 | 0.8 | 72.12 | 7.574 | 143.35 | 137.50 |
| G | 750 | 20 | 1 | 69.25 | 8.891 | 129.84 | 118.03 |
| H | 750 | 20 | 0.8 | 74.92 | 9.070 | 126.43 | 123.30 |
| I | 900 | 40 | 1 | 68.40 | 8.574 | 121.65 | 113.54 |
| J | 900 | 40 | 0.8 | 71.55 | 7.802 | 44.14 | 35.15 |
| K | 900 | 60 | 0.9 | 75.55 | 8.163 | 35.19 | 28.88 |
| L | 900 | 20 | 0.9 | 80.82 | 7.957 | 138.93 | 138.05 |
| M | 1000 | 40 | 0.9 | 66.35 | 10.539 | 94.83 | 35.34 |
| N | 750 | 40 | 0.9 | 68.62 | 10.729 | 117.58 | 55.44 |
| O | 900 | 40 | 0.9 | 73.95 | 8.078 | 122.39 | 120.29 |

3.4.1 Tensile strength before NAMLT

Figure 6a and Figure 6b show the typical stress-strain behavior of the specimen L and specimen K that exhibited the maximum and minimum tensile strength respectively. A maximum TS of 138.93 MPa was obtained in the specimen L that was FSWed at TTS of 20 mm/min, TRS of 900 rpm and TMR of 0.9.

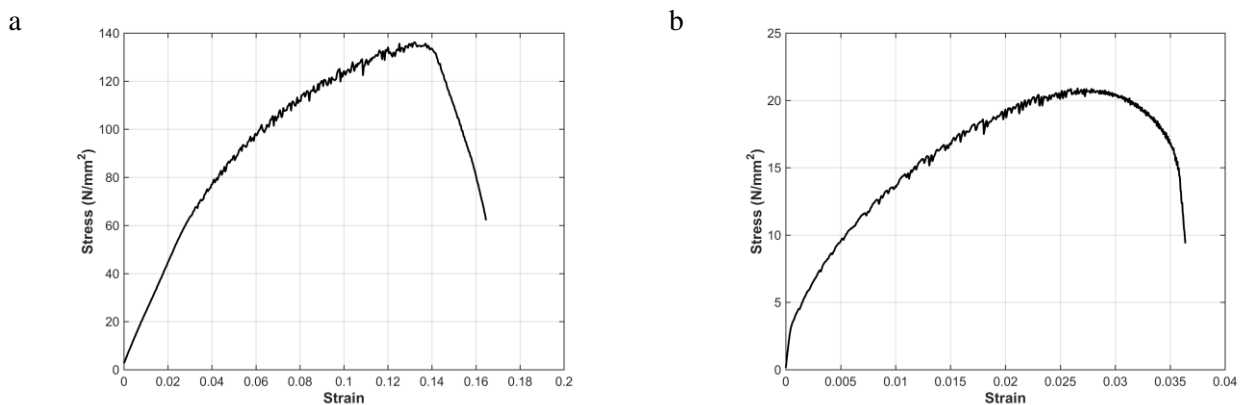


Figure 6 Typical Stress-Strain graph a) Specimen L (TRS- 900rpm, TTS- 20mm/min, TMR- 0.9) that had maximum TS; b) Specimen K (TRS- 900rpm, TTS- 60mm/min, TMR- 0.9) that had minimum TS

The hybrid model for predicting the TS of the FSWed specimens is given by equation (3). The contour plots that were generated using the model to study the effect of process parameters on the tensile strength of the FSWed specimens is shown in Figure 7. The influence of TRS and TMR on the tensile strength is shown in Figure 7a. It is observed that FSW of the specimen at TRS greater than 900 rpm and TMR below 0.86 resulted in low tensile

strength, while TRS within 800 & 900 rpm and TMR ranging between 0.87 & 0.99 resulted in high tensile strength.

$$\text{Tensile Strength} = -91.7106 - 31.7782 \times \text{TMR} + 35.7247 \times \text{TRS} - 25.0308 \times \text{TTS} - 44.2853 \times \text{TMR}^2 - 50.2595 \times \text{TRS}^2 - 0.438861 \times \text{TTS}^2 + \text{RBF Network using a multiquadric kernel with 4 centres, a global width of 0.33777, and regularization parameter, lambda is 0.0001.} \quad (3)$$

As shown in Figure 7b, FSW of the specimen at TRS above 900 rpm and TTS between 20 mm/min and 50 mm/min resulted in low tensile strength. In case of FSW of specimens at TRS between 800 rpm and 900 rpm, and TTS between 57 mm/min and 60 mm/min resulted in high tensile strength. From Figure 7c, it is observed that FSW at TTS in the range of 20 mm/min to 45 mm/min and TMR less than 0.88 resulted in low tensile strength. A high tensile strength was observed in the specimen FSWed at TTS between 57 mm/min and 60 mm/min, and TMR between 0.84 – 0.94. The optimum range of FSW process parameters that were inferred from the contour plots are as follows: TRS between 800 rpm and 900 rpm; TTS between 57 mm/min and 60 mm/min; TMR between 0.87 – 0.94. The maximum tensile strength that could be obtained by FSW at this level of process parameters would be 130 MPa to 170 MPa.

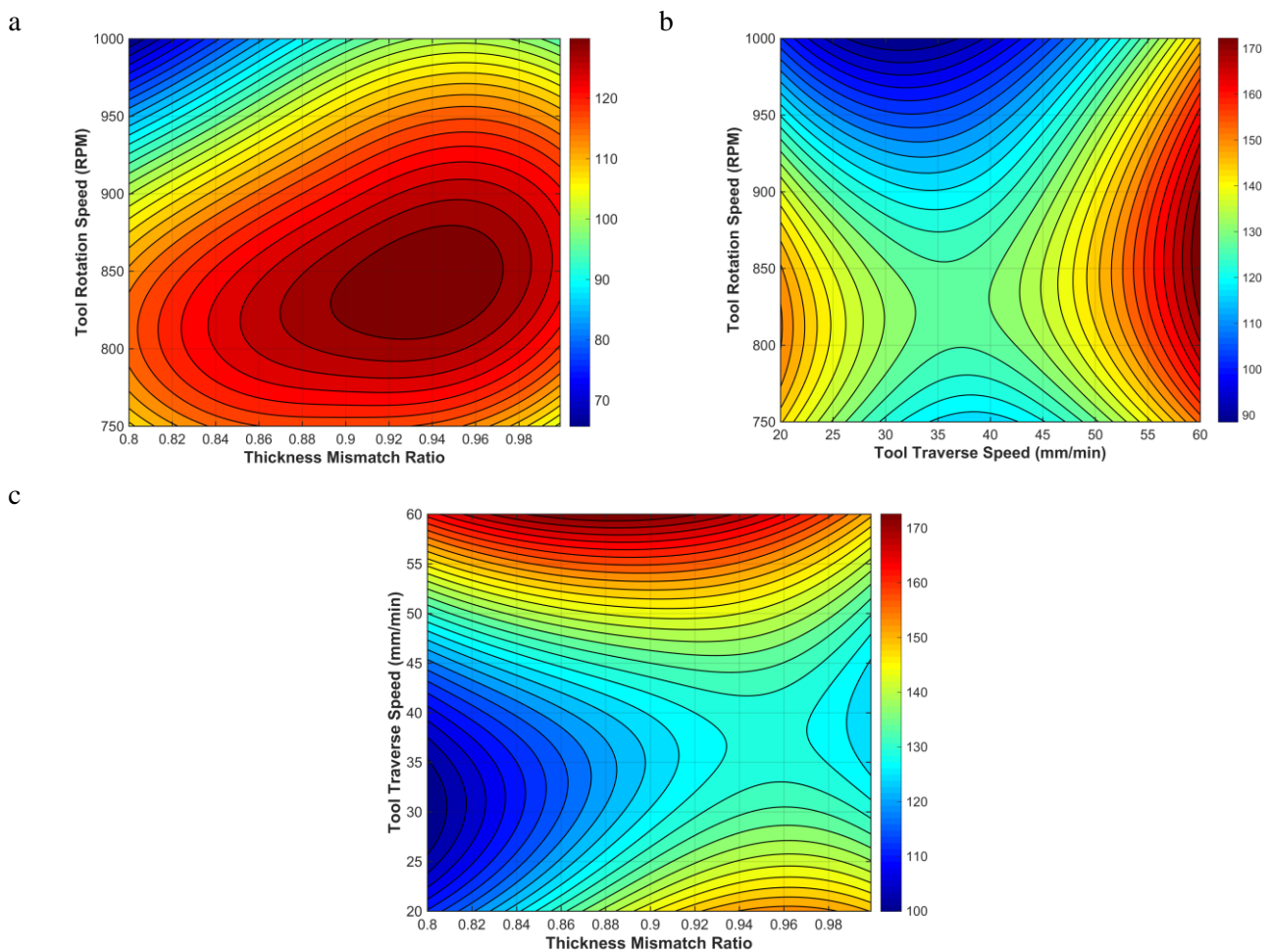


Figure 7 Contour plots showing the effect of a) TRS & TMR b) TRS & TTS and c) TTS & TMR on TS before NAMLT

The fractography of the specimen L that exhibited the highest tensile strength is shown in Figure 8. Figure 8a through Figure 8d shows the extensive plastic deformation (bright region) of the material before fracture. Besides, the fractography indicates more ductile fracture features (dimples) and secondary cracks. The plunging out of particles formed craters and pits (dark region), as observed in Figure 8a and Figure 8c.

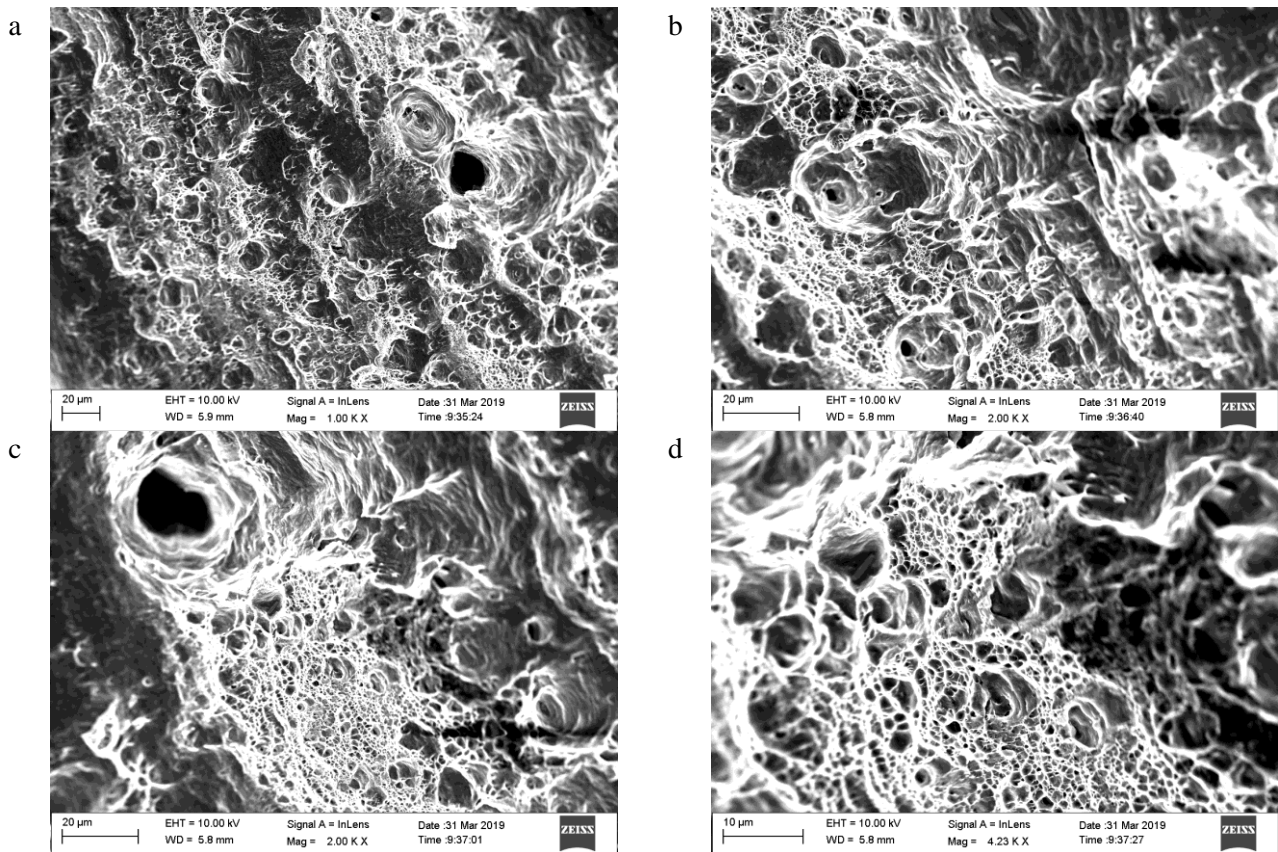


Figure 8 Fractography of the specimen L that was FSWed at TTS of 20 mm/min, TRS of 900 rpm and TMR of 0.9

3.4.2 Tensile Strength (after NAMLT)

The average tensile strength of the specimens after the NAMLT are shown in Table 4. The maximum TS of corrosion tested specimens was found to be 138.05MPa for the specimen L which was FSWed at TTS of 20 mm/min, TRS of 900rpm and TMR of 0.9. Figure 9a and Figure 9b show the stress-strain graphs of the specimen L and specimen D, which had the highest and the least tensile strength respectively.

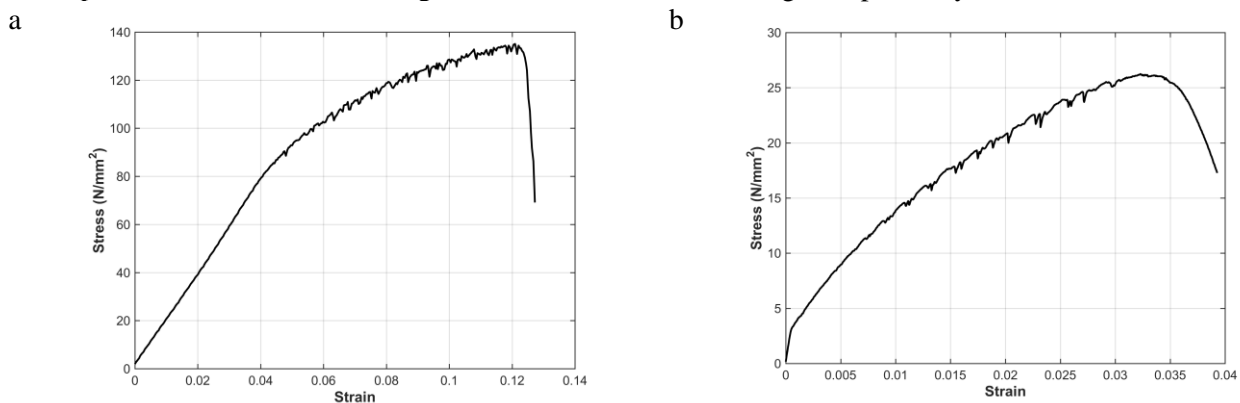


Figure 9 Typical Stress vs. Strain graph a) Specimen L (TRS- 900rpm, TTS- 20mm/min, TMR- 0.9) that had maximum TS after NAMLT; b) Specimen D (TRS- 1000rpm, TTS- 20mm/min, TMR- 0.8) that had minimum TS after NAMLT

The hybrid model for predicting the tensile strength (after NAMLT) of the friction stir welded specimens is given by the equation (4). The model was used to study the effect of process parameters on the tensile strength of the friction stir welded specimens

$$\text{Tensile Strength after NAMLT} = 124.2108 + 58.39332 \times \text{TMR} + 25.34766 \times \text{TRS} + 81.22661 \times \text{TTS} \quad (4) \\ + 11.92192 \times \text{TMR}^2 - 27.61802 \times \text{TRS}^2 + 57.96975 \times \text{TTS}^2 + \text{RBF Network using a multiquadric kernel} \\ \text{with 4 centres and a global width of 0.00011911, and regularization parameter, lambda is 0.0001.}$$

The influence of TRS and TMR on the tensile strength is shown in Figure 10a. It is observed that FSW of the specimen at TRS greater than 950 rpm and TMR between 0.80 and 0.90 resulted in low tensile strength after NAMLT, while TRS within 850 & 950 rpm and TMR ranging between 0.88 & 0.92 resulted in high tensile strength after NAMLT. As shown in Figure 7b, FSW of the specimen at between 750 rpm and 900 rpm and TTS between 20 mm/min and 30 mm/min resulted in high tensile strength after NAMLT. In the case of FSW of specimens at any TRS and TTS between 35 mm/min and 60 mm/min resulted in low tensile strength after NAMLT. From Figure 7c, it is observed that FSW at TTS in the range of 20 mm/min to 30 mm/min and TMR greater than 0.84 resulted in high tensile strength after NAMLT. A low tensile strength was observed in the specimen FSWed at TTS between 30 mm/min and 60 mm/min, and TMR between 0.80 – 0.90.

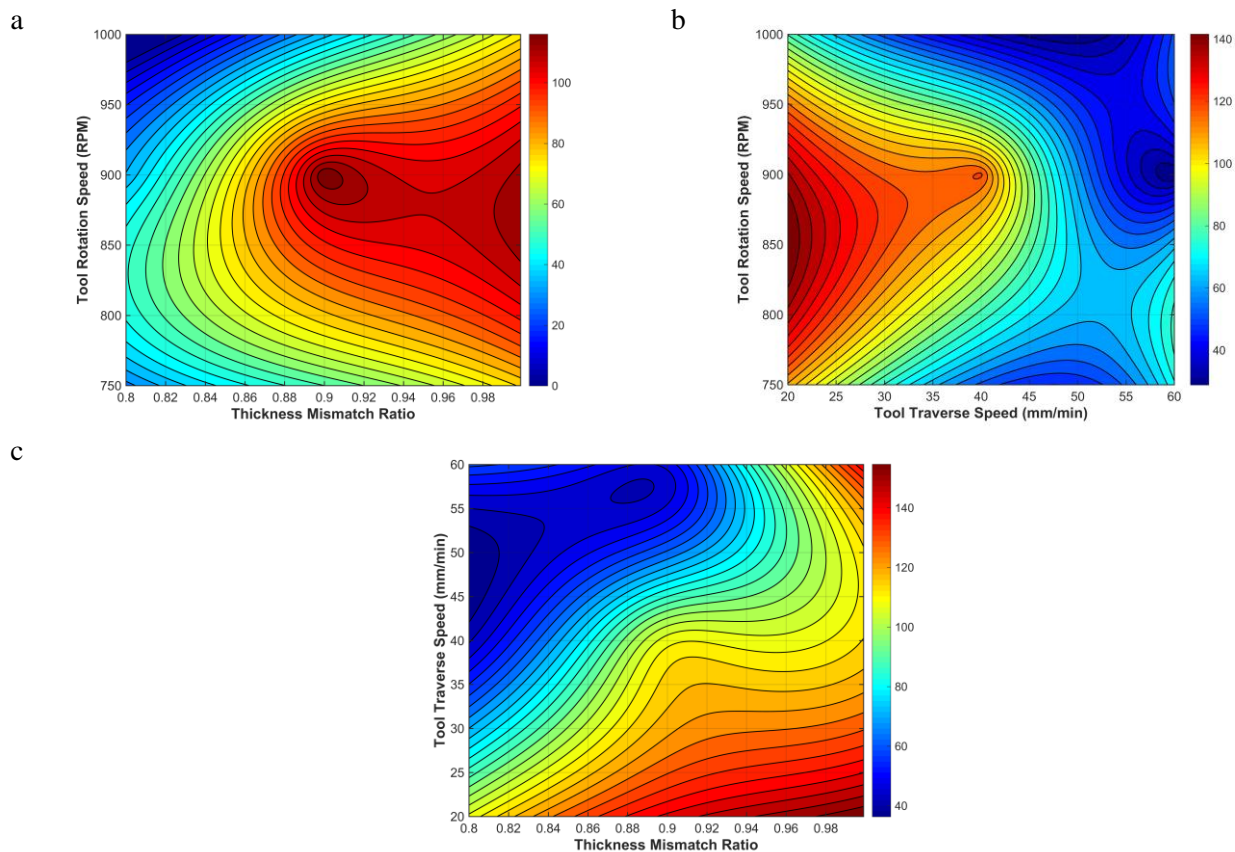


Figure 10 Contour plots showing the effect of a) TRS & TMR b) TRS & TTS and c) TTS & TMR on Tensile Strength after NAMLT

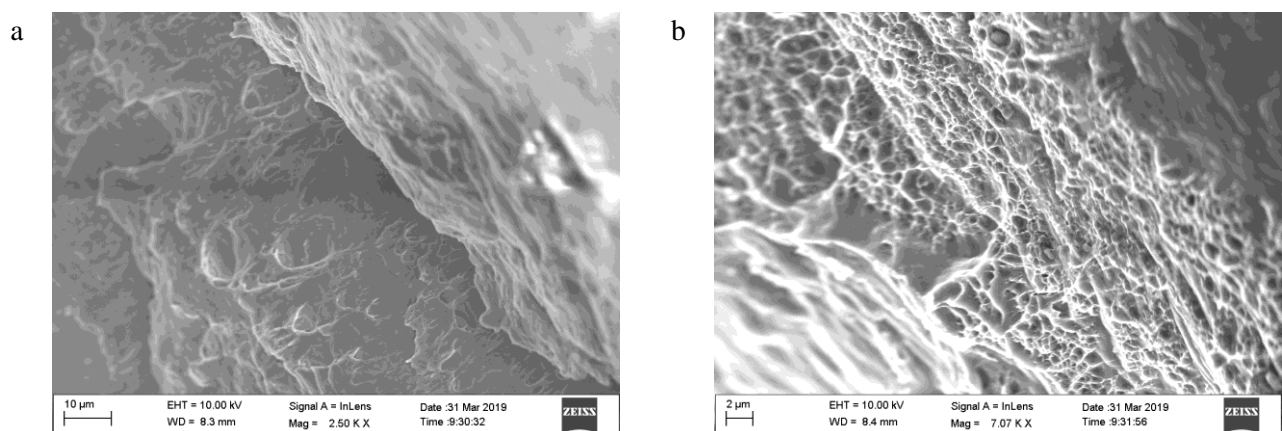


Figure 11 Fractography images showing A - Cracks B - Quasi-Cleavage C - Deformation zone

The optimum range of FSW process parameters that were inferred from the contour plots are as follows: TRS between 800 rpm and 900 rpm; TTS between 20 mm/min and 25 mm/min; TMR between 0.90 – 1.00. The maximum tensile strength that could be obtained by FSW at this level of process parameters would be 120 MPa to 150 MPa. The fractography of the specimen L that exhibited the highest tensile strength is shown in Figure 8. The fractograph indicated that no significant change was observed in the fracture mechanism in the specimen L after NAMLT.

Conclusion

Tailor welded blanks of AA5052 alloy were successfully produced by friction stir welding process. The microhardness and tensile strength of the welded specimens were evaluated. NAMLT test was performed on the specimens and the influence of corrosion on the tensile strength of the joints was evaluated. Hybrid RBF Quadratic Models were developed to interrelate the effect process parameters on the results (microhardness, NAMLT, tensile strength –before and after NAMLT). The outcomes proved that the TRS, TTS, and TMR are essential parameters in FSW of tailor welded blanks in AA5052 alloy. The deduced level of process parameters to produce better joints are as follows:

- Microhardness (72 - 76 HV): TRS of 750 - 850 rpm, TTS of 57 - 60 mm/min and TMR of 0.92 - 1.00
- mass loss per unit area ($8 - 8.5 \times 10^{-3}$ g/cm²): TRS of 800 - 950 rpm, TTS of 55 - 60 mm/min and TMR of 0.96 - 1.00
- Tensile Strength (130 - 170 MPa): TRS of 800 - 900 rpm, TTS of 57 - 60 mm/min and TMR of 0.87 - 0.94
- Tensile Strength after NAMLT (120 - 150 MPa): TRS of 800 - 900 rpm, TTS of 20 - 25 mm/min and TMR of 0.9 - 1.00

References

1. J. Benedyk, "Aluminum alloys for lightweight automotive structures," in *Materials, design and manufacturing for lightweight vehicles*, ed: Elsevier, 2010, pp. 79-113.
2. P. Kah, R. Rajan, J. Martikainen, and R. Suoranta, "Investigation of weld defects in friction-stir welding and fusion welding of aluminium alloys," *International Journal of Mechanical and Materials Engineering*, 10 (2015) 26.
3. R. Vaira Vignesh, R. Padmanaban, and M. Datta, "Influence of FSP on the microstructure, microhardness, intergranular corrosion susceptibility and wear resistance of AA5083 alloy," *Tribology-Materials, Surfaces & Interfaces*, 12 (2018) 157-169.
4. E. Cetkin, Y. H. Çelik, and S. Temiz, "Microstructure and mechanical properties of AA7075/AA5182 jointed by FSW," *Journal of Materials Processing Technology*, 268 (2019) 107-116.
5. G. Çam and G. İpekoğlu, "Recent developments in joining of aluminum alloys," *The International Journal of Advanced Manufacturing Technology*, 91 (2017) 1851-1866.
6. R. S. Mishra and Z. Ma, "Friction stir welding and processing," *Materials science and engineering: R: reports*, vol. 50, pp. 1-78, 2005.
7. P. Threadgill, A. Leonard, H. Shercliff, and P. Withers, "Friction stir welding of aluminium alloys," *International Materials Reviews*, vol. 54, pp. 49-93, 2009.
8. R. S. Mishra, P. S. De, and N. Kumar, *Friction stir welding and processing: science and engineering*: Springer, 2014.
9. V. V. Ramalingam and P. Ramasamy, "Modelling corrosion behavior of friction stir processed aluminium alloy 5083 using polynomial: radial basis function," *Transactions of the Indian Institute of Metals*, 70 (2017) 2575-2589.
10. M. Paidar, A. Asgari, O. O. Ojo, and A. Saberi, "Mechanical Properties and Wear Behavior of AA5182/WC Nanocomposite Fabricated by Friction Stir Welding at Different Tool Traverse Speeds," *Journal of Materials Engineering and Performance*, 27 (2018) 1714-1724.
11. R. Nandan, T. DebRoy, and H. Bhadeshia, "Recent advances in friction-stir welding—process, weldment structure and properties," *Progress in materials science*, 53 (2008) 980-1023.
12. M. Merklein, M. Johannes, M. Lechner, and A. Kuppert, "A review on tailored blanks—Production, applications and evaluation," *Journal of Materials Processing Technology*, vol. 214, pp. 151-164, 2014.
13. M. A. Siddharth, R. Padmanaban, and R. V. Vignesh, "Simulation of Friction Stir Welding of Aluminium Alloy AA5052—Tailor Welded Blanks," in *International Conference on Intelligent Systems Design and Applications*, 2018, pp. 113-122.

14. K. Ramachandran, N. Murugan, and S. Shashi Kumar, "Study on dissimilar butt joining of aluminum alloy, AA5052 and high strength low alloy steel through a modified FSW process," in *Materials Science Forum*, 2015, pp. 278-281.
15. X. Wang, Y. Pan, and D. A. Lados, "Friction stir welding of dissimilar Al/Al and Al/non-Al alloys: a review," *Metallurgical and Materials Transactions B*, 49 (2018) 2097-2117.
16. R. V. Vignesh, R. Padmanaban, and K. Chinnaraj, "Soft computing model for analysing the effect of friction stir processing parameters on the intergranular corrosion susceptibility of aluminium alloy AA5083," *Koroze a ochrana materiálu*, 62 (2018) 97-107.
17. R. Akbari, S. Mirdamadi, A. Khodabandeh, and M. Paidar, "A study on mechanical and microstructural properties of dissimilar FSWed joints of AA5251–AA5083 plates," *International Journal of Materials Research*, 107 (2016) 752-761.
18. H. Lombard, D. Hattingh, A. Steuwer, and M. James, "Optimising FSW process parameters to minimise defects and maximise fatigue life in 5083-H321 aluminium alloy," *Engineering Fracture Mechanics*, 75 (2008) 341-354.
19. K. Sabitha, P. R. Reddy, A. Krishnaiah, and R. U. Kumar, "Evaluation of Mechanical Properties of Tailor Welded Sheet Metal Blanks," in *IOP Conference Series: Materials Science and Engineering*, 2018, p. 012061.
20. C. Chanakyan, P. D. Babu, M. Jenarathanan, and K. Jagathesh, "An Experimental Investigation on Mechanical Properties and Microstructure of Friction Stir Welding of AA5052," in *Applied Mechanics and Materials*, 2014, pp. 48-52.
21. A. I. H. Committee, *Properties and selection: nonferrous alloys and special-purpose materials vol. 2: Asm Intl*, 1990.
22. R. Anil Kumar, K. Pavan Sai, R. Vaira Vignesh, and N. Radhika, "Investigations on the Tribological Properties of Heat-Treated Copper Composite Using Hybrid Quadratic–Radial Basis Function Model," *Transactions of the Indian Institute of Metals*, 2019/07/20 2019.
23. B. K. Murugan, V. Balusamy, R. Padmanaban, and R. V. Vignesh, "Study of the effect of parameters in friction surfacing of Monel over Mild Steel using linear–radial basis function model," *Materials Today: Proceedings*, 5 (2018) .
24. R. V. Vignesh and R. Padmanaban, "Influence of friction stir processing parameters on the wear resistance of aluminium alloy AA5083," *Materials Today: Proceedings*, 5 (2018) 7437-7446, 2018.
25. V. Ebrahimzadeh, M. Paidar, M. A. Safarkhanian, and O. Oladimeji Ojo, "Orbital friction stir lap welding of AA5456-H321/AA5456-O aluminum alloys under varied parameters," *The International Journal of Advanced Manufacturing Technology*, 96 (2018) 1237-1254.
26. N. Farmanbar, S. Mousavizade, and H. Ezatpour, "Achieving special mechanical properties with considering dwell time of AA5052 sheets welded by a simple novel friction stir spot welding," *Marine Structures*, 65 (2019) 197-214.
27. K. Kumar, S. V. Kailas, and T. S. Srivatsan, "Influence of tool geometry in friction stir welding," *Materials and Manufacturing Processes*, 23 (2008) 188-194.

(2019) ; <http://www.jmaterenvironsci.com>